Transparent conductive oxide films for high performance dye-sensitized solar cells

Umer Mehmood[1], Mohammad Afzaal, Amir Al-Ahmed, Heather M. Yates, Abbas S. Hakeem

Greek

Abstract-- **In this work, atmospheric pressure chemical vapor deposition of fluorine doped tin oxide (FTO) thin films of various thicknesses and dopant levels is reported. The deposited coatings used to fabricate dye-sensitized solar cells which exhibited reproducible power conversion efficiencies in excessive of 10%. No surface texturing of FTOs or any additional treatment of dye covered films is applied. In comparison, use of commercial FTOs showed a lower cell efficiency of 7.11%. Detailed analysis showed that the cell efficiencies do not simply depend on the resistivity of FTOs but instead rely on a combination of carrier concentration, thickness, and surface roughness properties**.

***Index Terms*-- Fluorine doped tin oxide; carrier concentration; surface roughness; forward haze; open circuit voltage**

I. Introduction

Since the ground breaking work of O'Regan and Grätzel on dye-sensitized solar cells (DSSCs) in 1991 [1], the last two decades have seen tremendous progress at many facets of the technology, with record efficiencies approaching 14.7% [2]. Cost competitive, ease of large scale fabrication, and compatibility (as well as aesthetic features) with windows and polymer films have been the major contributing factors in the popularity of DSSCs. Upon light absorption, the electron injection from a dye sensitizer to the conduction band of a wide bandgap metal oxide occurs, followed by the transfer to a transparent conducting oxide (TCO). The oxidized dye is regenerated by accepting electrons from an electrolyte which subsequently diffuses toward the counter electrode and the reduction takes place [3].

Dr John Hodgkinson is gratefully acknowledged for useful discussions on film properties. UM and AA would like to thank Center of Research Excellence in Renewable Energy, KFUPM for the support

Umer Mehmood and Amir Al-Ahmed belong to Center of Research Excellence in Renewable Energy, King Fahd University of Petroleum & Minerals, Dhahran, 31261, Saudi Arabia (umermehmood@kfupm.edu.sa, aalahmed@kfupm.edu.sa)
Mohammad Afzaal and Heather M. Yates are with Materials and Physics Research Centre, The University of Salford, Manchester, M5 4WT, United Kingdom (M.Afzaal@salford.ac.uk, H.M.Yates@salford.ac.uk)

Abbas S. Hakeem is with Center of Research Excellence in Nanotechnology, King Fahd University of Petroleum & Minerals, Dhahran, 31261, Saudi Arabia (ashakeem@kfupm.edu.sa)

Power conversion efficiencies (PCE) of DSSCs depend on its component(s) and the device fabrication process. The attempts to improve PCEs as highlighted in recent work has focused on the photoanodes, sensitizing materials, counter electrodes and redox electrolytes [4]–[7]. Less attention has been directed towards TCOs with suitable characteristics such as smooth surface morphologies, low resistivity and high transparency, possibly due to competing properties required for high performance DSSCs. In general, fluorine doped tin oxide (FTO) has been a common choice of TCO as opposed to tin doped indium oxide (ITO), due to its greater thermal stability [8] and lower costs. To enhance the surface roughness and hence the associated light scattering of FTOs surfaces, etching and nanopatterning of electrodes has been performed to achieve desired morphologies. However, the PCE remains between 6-8 % [9]–[14]. It is worth emphasising that highly textured FTO surfaces are considered an advantage for amorphous silicon (Si) based solar cells, due to their superior light scattering and trapping properties as Si is a poor absorber of light. For DSSCs, smooth FTO surfaces, *i.e*., low root mean square (RMS) roughness for a limited film thickness is desired, without sacrificing functional (optical and electrical) properties considerably. This would aid with the deposition of uniform blocking and/or sensitizer layers and increase the amount of light reaching the dye and generating the maximum number of excitons. Very recently, Park et al. have emphasised the significance of smooth films for perovskite solar cells for improving physical contact between FTO surfaces and electron transporting layers [15]. As a result, significant improvements in effective electron extraction and hole-blocking layers were noticed.

Herein, we demonstrate high-quality FTO thin films using a highly favourable atmospheric-pressure chemical vapour deposition (APCVD) process which allows accurate control over the processing conditions and yields films with a range of characteristics. The technique itself has significant attractions for deposition of the underlying TCO layer due to its compatibility with high volume and low cost production. As-deposited films are validated as TCOs for the assembly and characterization of DSSCs using a N3 dye, (cis-diisothiocyanato-bis(2,2'-bipyridyl-4,4'-dicarboxylic acid) ruthenium(II)) which demonstrated reproducible PCEs of over 10% through a large short circuit current density (Jsc) of $\approx$ 25 mA/cm^2 and fill factor (FF) $<$ 55%. The work highlights two significant improvements from previous attempts. Firstly, no change

of any sort is made to the FTO surfaces and thus, eliminating the use of any challenging or expensive surface modification procedures. Secondly, high efficiency DSSCs are feasible via a balance of film thickness and doping related properties. We expect that FTOs with improved properties will have important implications in modern solar cells and at the same time will find usage in electronics currently dominated by expensive and scarce ITO.

II. EXPERIMENTAL

All the chemicals were purchased from Sigma Aldrich Ltd and used as received. The dye was acquired from Solaronix Ltd. Prior to conducting deposition experiments, 1.1 mm borosilicate glass substrates (Corning Eagle 2000) were cleaned with detergent, water, propan-2-ol, and dried in air. The system was purged under constant nitrogen (N_2) for few hours, before carrying out any coatings.

A. Preparation of Thin Films

SnO_2:F thin films were deposited by APCVD at 600 °C using monobutyltin trichloride (MBTC) with 0.2 – 1.0 M aqueous trifluoroacetic acid (TFAA) solution. During coating experiments, Sn precursor to water (H_2O) molar ratio was fixed at 1:5. The precursors were vapourised using either bubbler (MBTC at 125 °C, 0.6 l/min^{-1} carrier gas) or flash evaporation (TFAA/H_2O mix, 0.7 l min^{-1} carrier gas). N_2 used as the carrier gas was mixed with oxygen (1.5 l/min^{-1}). An APCVD gas handling system combined with an in-house designed coater head system was used to deliver precursors to the substrate surface. The heated substrate was translated on an automated stage, beneath a static, non-contact gas distributor in an extracted, open atmosphere, enclosure. This allowed the deposition of films over 10 cm ×10 cm area with good uniformity (± 2%). The number of substrate passes (4, 6 or 8) under the coating head were adjusted to deposit films of multiple thicknesses.

B. Device Fabrication

Photoanodes were prepared with an area of 0.2 cm^2 by tape casting method. TiO_2 paste was casted on the pre-cleaned FTO glass substrates (1.5 cm^2) and was heated on a hotplate at 450 °C for 30 mins, which resulted in 8 µm thick films. After cooling to room temperature, these TiO_2 coated substrates were soaked in 0.5 mM solution of N3 dye, (cis-diisothiocyanato-bis(2,2'-bipyridyl-4,4'-dicarboxylic acid) ruthenium(II)) in methanol for 24 hrs to absorb the dye onto the TiO_2 surface [16], [17]. This ensured good coverage and loading of N3 onto the TiO_2 electrodes and induced electronic coupling between the dye and the TiO_2 for efficient charge injection. After the dye absorption, TiO_2/FTO samples were taken out and washed gently with ethanol to remove any unanchored dye. Platinum paste was tape casted on FTO substrates and annealed at 450 °C for 15 min over a hot plate to prepare the counter electrode (FTO/Pt). Cells FTO/Pt-(Dye)TiO_2/FTO) were assembled by joining both the electrodes using a super glue. Finally, an electrolyte was inserted into the cell using a dropper to complete the cell fabrication.

III. RESULTS AND DISCUSSION

Thin films of FTOs were deposited with varying fluorine dopant concentrations and thicknesses. The coatings had good coverage and were strongly adhered to the surfaces. A summary of resulting film properties is given in Table 1. Increasing the number of passes under the coating head demonstrated the expected approximately linear increase in film thicknesses. For example, film thicknesses ranged between 0.46 – 0.82 µm by changing the number of passes from 4 to 8 for 0.2M TFAA samples (Figure 1a).

A. X-ray powder diffraction (XRD) analysis

The X-ray powder diffraction (XRD) exclusively showed the formation of polycrystalline SnO_2 films with a tetragonal structure, (JCPDS No: 021-1250) without any Sn or SnO impurities (Figure 2a, supporting information S1 and S2). One noticeable difference between the diffraction patterns was the crystallite size which increased with film thickness. This could possibly be attributed to continuation crystal growth along the same plane with prolonged growth times. To demonstrate the effect, crystallites sizes jumped from 18 to 44 nm as the film thickness (*via* number of passes) increased from 590 nm to 916 nm for the 0.6 M samples (Table 1). The size differences depended on the doping levels and were more pronounced for 0.2M TFAA samples (Figure 1b). Irrespective of doping concentrations, films showed a preferred orientation along the (200) plane of tetragonal SnO_2. More significantly, the texture coefficient (TC) value for the (200) peak increases with the film thicknesses which in turn implies that the number of particles having a (200) preferred orientation increased with the number of passes and hence film thickness (Figures 2a, supporting information S1 and S2).

TABLE I

Properties of as-deposited FTO thin films.

Sample no	TFAA concentration/M	No of passes	*d* (μm)	RMS roughness (nm)	Crystallite size (nm)	*TC*	Sheet resistance (Ω/sq)	$\rho/\times10^{-3}$ (Ω/cm)	μ (cm^2/Vs)	$N/\times10^{20}$ (cm^{-3})	*H* (%) 450 nm	*T* (%) 531 nm
S1	0.2	4	0.457 ± 0.023	19	32	3.77	61.4	2.81	20	0.72	1.3	88
S2	0.2	6	0.721 ± 0.013	19	37	3.89	24.9	1.80	20	2.0	0.8	82
S3	0.2	8	0.823 ± 0.010	28	53	3.31	16.7	1.37	24	1.7	0.9	80
S4	0.6	6	0.590 ± 0.006	22	18	3.84	17.7	1.04	20	3.2	2	85
S5	0.6	8	0.916 ± 0.032	28	44	3.85	11.2	1.03	24	3.3	1.1	81
S6	1	6	0.648 ± 0.026	25	41	3.56	10	0.65	21	4.6	1.2	83
S7	1	8	0.771 ± 0.034	28	42	3.97	7	0.54	24	5.3	0.6	82
TCO7			0.58	23	32	2.12	7	0.41				>70*

d: Average film thickness, AFM – root mean squared (RMS) roughness, *TC*: texture coefficient, *ρ:* resistivity, *μ*: mobility, *N*: carrier concentration, *H*: haze, *T*: transmission. TCO7 refers to commercial Solaronix TCO22-7 substrate. * denotes transmission between 470-1100 nm.

B. SEM and AFM Analyses

Scanning electron microscope images showed the formation of compact granular or pyramidal structural features, depending on the dopant levels and film thicknesses (supporting information S3). The samples S1-S5 were predominantly pyramidal whereas S6 and S7 consisted of granular type morphologies. Further characterisation by atomic force microscopy (AFM) revealed RMS values which vary significantly between films (Figures 2b and supporting information S4). In general, as previously seen that the surface roughness increases (high RMS values) with increased thickness (Figure 1b) [18]. Only a marginal difference in RMS values is seen for sample 1 and 2. However, the true effect is manifested in the electrical and solar performance of the films, as discussed later. Interestingly, despite different sample roughnesses average particle heights estimated by full width half maximum of statistical analysis of AFM images were also very similar (46 and 44 nm for 4 and 6 passes, respectively). However, with a further increase in film thickness (to 8 passes), the value jumps to 66 nm (Figure 2c). This implies a wider range of surface height variation, which is in agreement with the increased surface roughness. Surface feature angles show a fairly broad distribution in line with the polycrystalline nature of the films. The position of the histogram maximum seems relatively unaffected by increased film thicknesses, as the values range only between 21-29° relative to the internal angle with the substrate (Figure 2d). One would expect smooth surface S1 to have the lowest angle but it actually has the highest. The thickest sample S3 does have a different distribution and is the most dissimilar in terms of grain size. This may relate to it containing much larger crystallites (than the other two samples), which impinge on each other causing a small amount of shape distortion and hence angle changes. For higher dopant levels such as 0.6 or 1M TFAA containing samples, the difference in feature heights and angles are less pronounced (supporting information S5).

C. X-ray photoelectron spectroscopy (XPS)

The chemical composition of two dissimilar FTO samples was compared by XPS. These were S2 with a low dopant level and S6 with a high dopant level. Both samples showed identical Sn 3d with the $3d_{5/2}$ at 486.8 eV and spin-orbital splitting, Δ= 8.4 eV, which can be assigned to tin oxide (Figure 3) [19]. This was confirmed from the O 1s, which could be resolved into two signals, the most intense at 530.5 eV relating to O attached to a metal (Figure 3). The additional broader signal at 531.4 eV can be related to oxygen attached to carbon and/or hydroxyl groups [20]. In our samples this additional signal was of fairly low intensity (for S2 particularly) so probably related to surface impurities and absorbed water. The increased strength of this signal in S6 is combined with increased intensity of the C1s (and reduced intensity of the Sn 3d) so suggesting increased hydrocarbon surface impurities. However, the dominant C 1s signal was from adventitious C, used routinely as the calibration standard. As the XPS was done at a much later date than the FTO deposition it is feasible more surface contamination has occurred. The presence of any F from the dopant or impurity Cl from the precursor was not detected, being below the instrument detection

limits. Fitting the 3d and O1s peaks established the samples were relatively stoichiometric with S2 $SnO_{2.0}$ and S6 $SnO_{1.8}$ and potentially ruling out composition related effects in cell efficiencies.

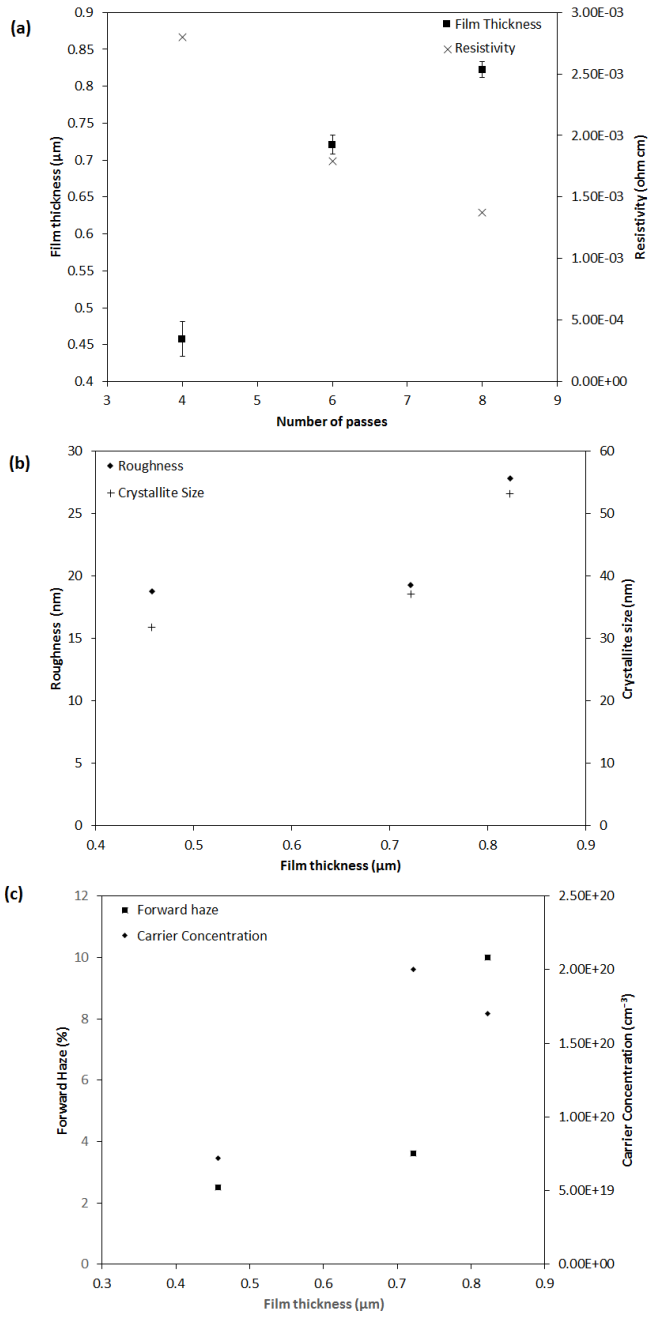

Fig. 1.(a) Film thickness and resistivity as a function of number of passes,(b) roughness and crystallite sizes, and (c) forward haze and carrier concentration as a function of film thickness. All the data is for 0.2M TFAA samples only.

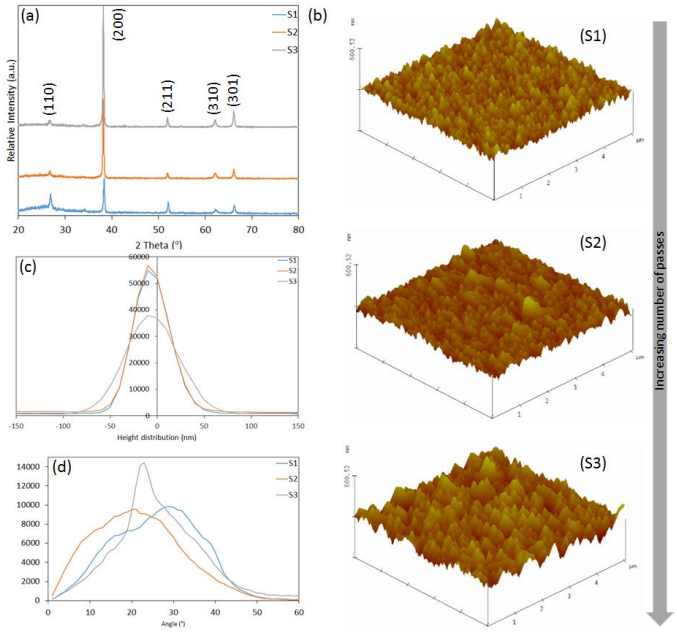

Fig. 2. (a) XRD patterns and (b) AFM images of S1-S3 (c) and (d) show statistical analysis of AFM data for S1-S3

D. Optical and Electrical Properties

Irrespective of dopant concentrations and film thicknesses, samples exhibited respectable transmittance > 80 % at a wavelength of 531 nm and thus, any associated absorption losses are minimized. As expected, a reduction in the transmission with increased film thicknesses or number of passes is also evident. Optical scattering (forward haze values) (at 531 nm) increased with film thickness and hence surface roughness. The values also changed with the dopant concentration although any correlation between the dopant levels and resulting haze properties is masked by the changes in film thickness. In terms of resistivity (ρ), all the samples are highly resistive, with the lowest values (5.4 and 6.48 × 10^{-4} Ω/cm) seen for S6 and S7. Hall Effect meaurements surprisingly yielded similar mobility values, 24 cm^2/Vs for all the thick samples which reduced to 20 or 21 cm^2/Vs as the films became thinner. The greater mobility for thicker samples is a direct result of their larger crystallite sizes and reduced number of grain boundaries. Otherwise, potential barriers introduced by the increased gaps or discontinuity between the small grains would result in scattering of crossing electrons and yield poor charge mobility. The majority of the samples exhibited carrier concentrations (N) in the region of 10^{20} cm^{-3}, associated with scattering mechanisms within the bulk properties of the films [21]. For S1, N is reduced to 7.2 × 10^{19} cm^{-3} and is possibly due to scattering processes at the grain boundaries (Figure 1c) [22].

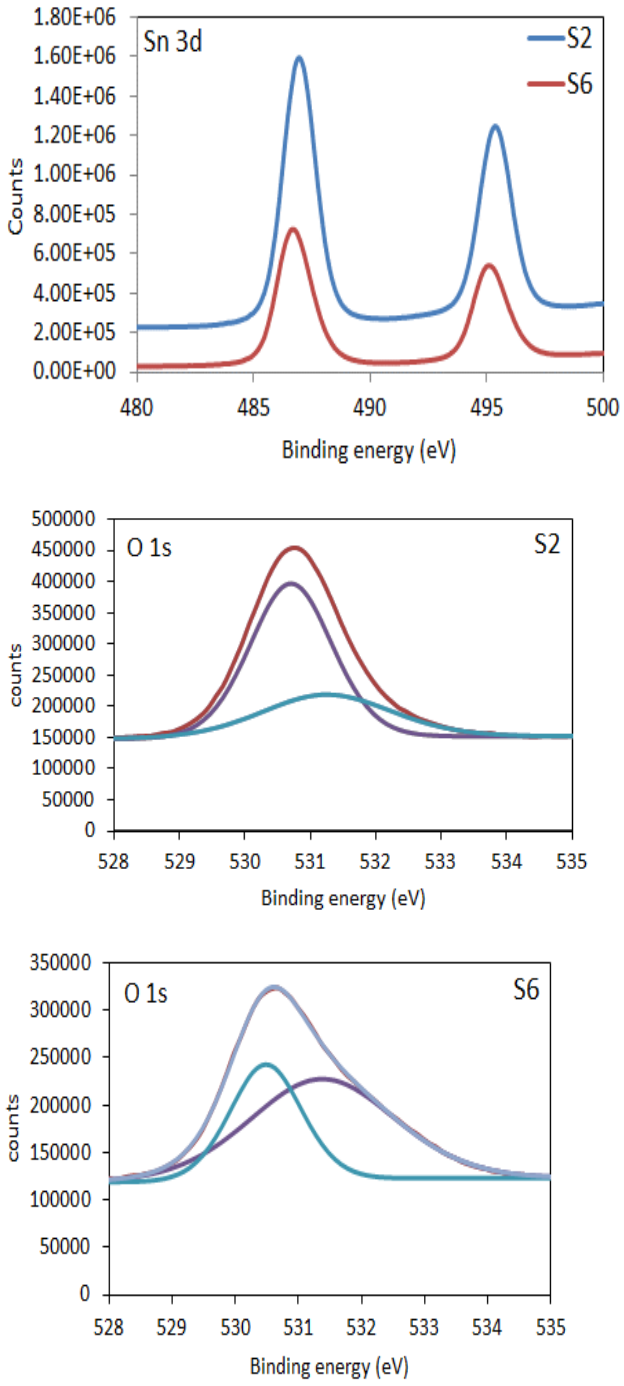

Fig. 3. XPS spectra of Sn 3d for S2 and S6 (top), O 1s for S2 (middle) and S6 (bottom)

E. Photovoltaic performance of DSSCs

As-prepared samples were utilized as TCOs for the fabrication and characterization of DSSCs involving ruthenium sensitizer, N3 often referred as first generation dye and compared with commercially available Solaronix TCO22-7 glass (Figure 4 and supporting information S7a). The photovoltaic performance of the DSSCs is summarized in Table 2. The four most efficient cells give PCE values significantly higher than reported efficiencies seen for treated and untreated N3 dye films [23], [24]. By looking at FTO properties (Table 1), our most efficent devices from S2 (ave. 10.3 %) do not depend on the resistivity of the substrates alone but instead rely on combined thickness and surface roughness related properties (haze and transmission). This balance is important as the improvement of one property leads to the reduction in another required property. For example a smooth film with high optical transmission would be of higher resistivity. To reduce the resistivity the film either needs to be thicker (and hence lower transmission and rougher) or more highly doped (which again reduces the transmission). The over-ridding property for S2 seems to be its increased smoothness, lower haze coupled with its relatively low carrier concentration and not its relatively high sheet resistance. For example, the cell values for S1 and the reference TCO7 are very similar despite the very large difference in FTO resistance. The advantage for the TCO7 being its low sheet resistance, while the disadvantages (compared to S1) being its large RMS (~23 nm), increased film thickness (0.58 μm) and significantly reduced TC (2.12) along the (200) plane. An AFM image and XRD pattern of commercial TCO7 is given in supporting information S6. Again, S1 despite being smoother than other coated samples, it exhibited lowest PCE due to very high ρ and reduced N. An increase in the sheet resistance from an optimum limit retards the charge transport and therefore yields low current density as evident in the case of S1. It was observed that high series resistance (R_s) and low shunt resistance (R_{sh}) mainly contributed to low FF (Table 2). Low R_{sh} causes power losses by providing an alternate pathway for the light-generated current and reduces FF. High R_s and low R_{sh} are mainly due to the fabrication defects occurred during the cell fabrication such as fast drying of electrode, thick electrolyte layer or platinum back contact [25]–[27]. FTO films have a particular set of properties due to employed growth conditions and thus are expected to have knock-on effects on the J_{sc} values. Relative to other samples, S1 and S4 have low J_{sc} than 19 mA/cm^2, due to high sheet resistance and small crystallite sizes (increased recombination at grain boundaries), respectively [13], [28]. Large particles sizes are preferred for minimising grain boundary recombination which result in improved improve electron transport on the FTO surface and the interfacial pathway between the TiO_2 layer and the FTO film.

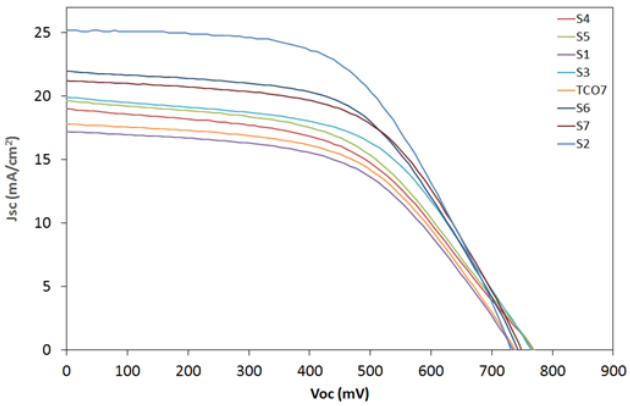

Fig.4.The photocurrent-voltage of DSSCs based on as-deposited FTO thin films under Am 1.5 G illuminations.

TABLE II
Photovoltaic properties of DSSCs

Sample no	J_{sc} (mA/cm^2)	V_{oc} (V)	FF (%)	R_s (Ω cm$^{2)}$	R_{sh} (Ω cm^2)	PCE (%)
S1	17.195	0.735	53.94	75.00	408	6.82
S2	25.121	0.732	55.78	62.00	936	10.20
S2*	25.305	0.733	56.00	61.00	947	10.40
S2**	25.127	0.730	55.97	61.00	946	10.30
S3	19.933	0.765	53.71	70.42	374	8.19
S4	18.981	0.768	50.64	87.00	300	7.38
S5	19.630	0.769	50.85	85.00	284	7.68
S6	21.947	0.742	55.32	59.53	288	9.02
S7	21.206	0.749	56.20	58.50	470	8.92
TCO7	17.797	0.738	54.11	72.46	404	7.11

F. Electrochemical impedance spectroscopy (EIS) analysis

Electrochemical impedance spectroscopy (EIS) to measure the current response at different frequencies of the applied AC voltage was used to study the charge transfer resistance of the cells. The Nyquist plots for the DSSCs studied and the equivalent circuit are shown in Figure 5. Typically, a normal EIS of DSSCs consists of three arcs (semicircles) [29]. The first semicircle represents the interfacial resistance at the counter electrode/electrolyte interface (R_2), second shows the interfacial resistance at the photoanode/electrolyte interface (R_3) or (*Rct*), and the third exhibits the impedance due to the diffusion process of I^-/I_3^- redox couple in the electrolyte (*Zw*). Only the second arcs appear in the Nyquist plots. It is probable that the first and third arc corresponding to R_2 and *Zw* are overshadowed by the large semicircle representing R_3 [30], [31]. The R_3 is related to the charge recombination rate, i.e. a large R_3 indicates a slower charge recombination and a longer electron lifetime. It is clearly evident in Figure 5 and supporting information S7b that the R_3 of cell prepared with all S2 samples (which gave the most efficient cells) is ave. 161.67Ω and is much higher than all other cells. This higher R_3 value is responsible for the slower charge recombination, injection of electrons towards TiO_2 conduction band and a reduction in dark current. All these attributes result in higher cell efficiencies. Table 3 shows the R_3 values of all the samples.

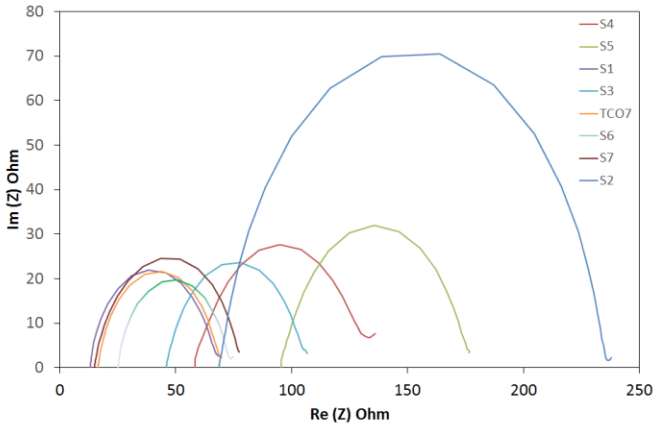

Fig.5. EIS curves of DSSCs based on as-deposited FTO thin films. Inset in bottom shows the equivalent circuit used to fit the experimental data. TCO7 refers to commercial Solaronix TCO22-7 substrate.

TABLE III
Charge combination resistance at TiO_2/dye/electrolyte interface of DSSCs. * and ** indicates reproducible cell values for S2. TCO7 refers to commercial Solaronix TCO22-7 substrate.

Sample no	R_3 (Ω)
S1	53.32
S2	144
S2*	166
S2**	155
S3	63.78
S4	72.67
S5	80.03
S6	58.08
S7	63.15
TCO7	55.78

IV. CONCLUSION

In conclusion, we have successfully demonstrated that power conversion efficiencies of DSSCs can notably be improved by adjusting FTO film properties, without the need of any surface treatment(s). Our investigations clearly demonstrate the importance of combined film properties and their contribution towards high performance photovoltaic cells through increased fill factor and short circuit currents. To deposit FTO films with a range of characteristics, an APCVD system with a fixed translation speed under the coating head was exploited. This has the potential to major impact on a range of efficient optoelectronic devices requiring abundant and affordable TCO

V. ACKNOWLEDGMENT

The authors would like to acknowledge the Center of Research Excellence for Renewable Energy at KFUPM for providing the lab facility.

VI. REFERENCES

[1] B. O'Regan and M. Grätzel, "A low-cost, high-efficiency solar cell based on dye-sensitized colloidal TiO2 films," *Nature*, vol. 353, no. 6346, pp. 737–740, Oct. 1991.

[2] K. Kakiage, Y. Aoyama, T. Yano, K. Oya, J. Fujisawa, and M. Hanaya, "Highly-efficient dye-sensitized solar cells with collaborative sensitization by silyl-anchor and carboxy-anchor dyes.," *Chem. Commun. (Camb).*, vol. 51, no. 88, pp. 15894–7, Nov. 2015.

[3] M. Grätzel, "Recent advances in sensitized mesoscopic solar cells.," *Acc. Chem. Res.*, vol. 42, no. 11, pp. 1788–98, Nov. 2009.

[4] Y. Yasu, T. Koike, and M. Akita, "Intermolecular aminotrifluoromethylation of alkenes by visible-light-driven photoredox catalysis.," *Org. Lett.*, vol. 15, no. 9, pp. 2136–9, May 2013.

[5] F. Bella, C. Gerbaldi, C. Barolo, and M. Grätzel, "Aqueous dye-sensitized solar cells.," *Chem. Soc. Rev.*, vol. 44, no. 11, pp. 3431–73, Jun. 2015.

[6] A. Hagfeldt, G. Boschloo, L. Sun, L. Kloo, and H. Pettersson, "Dye-sensitized solar cells.," *Chem. Rev.*, vol. 110, no. 11, pp. 6595–663, Nov. 2010.

[7] M. Ye, X. Wen, M. Wang, J. Iocozzia, N. Zhang, C. Lin, and Z. Lin, "Recent advances in dye-sensitized solar cells: from photoanodes, sensitizers and electrolytes to counter electrodes," *Mater. Today*, vol. 18, no. 3, pp. 155–162, Apr. 2015.

[8] T. Kawashima, T. Ezure, K. Okada, H. Matsui, K. Goto, and N. Tanabe, "FTO/ITO double-layered transparent conductive oxide for dye-sensitized solar cells," *J. Photochem. Photobiol. A Chem.*, vol. 164, no. 1–3, pp. 199–202, Jun. 2004.

[9] F. Wang, N. K. Subbaiyan, Q. Wang, C. Rochford, G. Xu, R. Lu, A. Elliot, F. D'Souza, R. Hui, and J. Wu, "Development of nanopatterned fluorine-doped tin oxide electrodes for dye-sensitized solar cells with improved light trapping.," *ACS Appl. Mater. Interfaces*, vol. 4, no. 3, pp. 1565–72, Mar. 2012.

[10] Z. Yang, S. Gao, W. Li, V. Vlasko-Vlasov, U. Welp, W.-K. Kwok, and T. Xu, "Three-dimensional photonic crystal fluorinated tin oxide (FTO) electrodes: synthesis and optical and electrical properties.," *ACS Appl. Mater. Interfaces*, vol. 3, no. 4, pp. 1101–8, Apr. 2011.

[11] Z. Yang, S. Gao, T. Li, F.-Q. Liu, Y. Ren, and T. Xu, "Enhanced electron extraction from template-free 3D nanoparticulate transparent conducting oxide (TCO) electrodes for dye-sensitized solar cells.," *ACS Appl. Mater. Interfaces*, vol. 4, no. 8, pp. 4419–27, Aug. 2012.

[12] T. Chih-Hung, H. Sui-Ying, H. Tsung-Wei, T. Yu-Tang, C. Yan-Fang, Y. H. Jhang, L. Hsieh, W. Chung-Chih, C. Yen-Shan, C. Chieh-Wei, and L. Chung-Chun, "Influences of textures in fluorine-doped tin oxide on characteristics of dye-sensitized solar cells," *Org. Electron.*, vol. 12, no. 12, pp. 2003–2011, Dec. 2011.

[13] N. Chantarat, Y.-W. Chen, S.-H. Hsu, C.-C. Lin, M.-C. Chiang, and S.-Y. Chen, "Effect of Oxygen on the Microstructural Growth and Physical Properties of Transparent Conducting Fluorine-Doped Tin Oxide Thin Films Fabricated by the Spray Pyrolysis Method," *ECS J. Solid State Sci. Technol.*, vol. 2, no. 9, pp. Q131–Q135, Jun. 2013.

[14] K. R. Catchpole, S. Mokkapati, F. Beck, E.-C. Wang, A. McKinley, A. Basch, and J. Lee, "Plasmonics and nanophotonics for photovoltaics," *MRS Bull.*, vol. 36, no. 06, pp. 461–467, Jun. 2011.

[15] J. Choi, S. Song, M. T. Hörantner, H. J. Snaith, and T. Park, "Well-Defined Nanostructured, Single-Crystalline TiO2 Electron Transport Layer for Efficient Planar Perovskite Solar Cells," 2016.

[16] M. K. Nazeeruddin, R. Humphry-Baker, P. Liska, and M. Grätzel, "Investigation of Sensitizer Adsorption and the Influence of Protons on Current and Voltage of a Dye-Sensitized Nanocrystalline TiO 2 Solar Cell," *J. Phys. Chem. B*, vol. 107, no. 34, pp. 8981–8987, Aug. 2003.

[17] A. Fillinger, "The Adsorption Behavior of a Ruthenium-Based Sensitizing Dye to Nanocrystalline TiO[sub 2] Coverage Effects on the External and Internal Sensitization Quantum Yields," *J. Electrochem. Soc.*, vol. 146, no. 12, p. 4559, Dec. 1999.

[18] F. F. H.M. Yates, P. Evans, D.W. Sheel, Z. Remes, M. Vanecek, U. Dagkaldiran, A. Gordijn, "Optimum performance solar cells using atmospheric pressure chemical vapour deposition deposited TCOs," *Int. J. Nanotechnol.*, vol. 6, no. 9, p. pp.816 – 827, 2009.

[19] R. C. K. J. Chastain, *Handbook of X – Ray photoelectron spectroscopy*. 1995.

[20] Y. Sun, T. Egawa, L. Zhang, and X. Yao, "Effect of Collection Distance on the Lattice Structure of Anatase Titania Nanoparticles Prepared by Metalorganic Chemical Vapor Deposition," *Jpn. J. Appl. Phys.*, vol. 41, no. Part 2, No. 12A, pp. L1389–L1392, Dec. 2002.

[21] M. vandendonker, A. Gordijn, H. Stiebig, F. Finger, B. Rech, B. Stannowski, R. Bartl, E. Hamers, R. Schlatmann, and G. Jongerden, "Flexible amorphous and microcrystalline silicon tandem solar modules in the temporary superstrate concept," *Sol. Energy Mater. Sol. Cells*, vol. 91, no. 7, pp. 572–580, Apr. 2007.

[22] C. D. Canestraro, M. M. Oliveira, R. Valaski, M. V. S. da Silva, D. G. F. David, I. Pepe, A. F. da Silva, L. S. Roman, and C. Persson, "Strong inter-conduction-band absorption in heavily fluorine doped tin oxide," *Appl. Surf. Sci.*, vol. 255, no. 5, pp. 1874–1879, Dec. 2008.

[23] T. Horiuchi, H. Miura, K. Sumioka, and S. Uchida, "High efficiency of dye-sensitized solar cells based on metal-free indoline dyes.," *J. Am. Chem. Soc.*, vol. 126, no. 39, pp. 12218–9, Oct. 2004.

[24] M. K. Nazeeruddin, A. Kay, I. Rodicio, R. Humphry-Baker, E. Mueller, P. Liska, N. Vlachopoulos, and M. Graetzel, "Conversion of light to electricity by cis-X2bis(2,2'-bipyridyl-4,4'-dicarboxylate)ruthenium(II) charge-transfer sensitizers (X = Cl-, Br-, I-, CN-, and SCN-) on nanocrystalline titanium dioxide electrodes," *J. Am. Chem. Soc.*, vol. 115, no. 14, pp. 6382–6390, Jul. 1993.

[25] L. Han, N. Koide, Y. Chiba, A. Islam, R. Komiya, N. Fuke, A. Fukui, and R. Yamanaka, "Improvement of efficiency of dye-sensitized solar cells by reduction of internal resistance," *Appl. Phys. Lett.*, vol. 86, no. 21, p. 213501, May 2005.

[26] P. Joshi, L. Zhang, Q. Chen, D. Galipeau, H. Fong, and Q. Qiao, "Electrospun carbon nanofibers as low-cost counter electrode for

dye-sensitized solar cells.," *ACS Appl. Mater. Interfaces*, vol. 2, no. 12, pp. 3572–7, Dec. 2010.

[27] and G. C. Qifeng Zhang, Tammy P. Chou, Bryan Russo, Samson A. Jenekhe, "Polydisperse Aggregates of ZnO Nanocrystallites: A Method for Energy-Conversion-Efficiency Enhancement in Dye-Sensitized Solar Cells," *Adv. Funct. Mater.*, vol. 18, pp. 1654–1660, 2008.

[28] H.-R. An, H. An, D.-H. Riu, and H.-J. Ahn, "Improved Photovoltaic Properties Of Dye-Sensitized Solar Cells Using Laser Patterned F-Doped SnO2 Thin Films," *Arch. Metall. Mater.*, vol. 60, no. 2, pp. 1241–1245, Jan. 2015.

[29] K. LEE, C. HU, H. CHEN, and K. HO, "Incorporating carbon nanotube in a low-temperature fabrication process for dye-sensitized TiO2 solar cells☆," *Sol. Energy Mater. Sol. Cells*, vol. 92, no. 12, pp. 1628–1633, Dec. 2008.

[30] S. Li, Y. Lin, W. Tan, J. Zhang, X. Zhou, J. Chen, and Z. Chen, "Preparation and performance of dye-sensitized solar cells based on ZnO-modified TiO2 electrodes," *Int. J. Miner. Metall. Mater.*, vol. 17, no. 1, pp. 92–97, Feb. 2010.

[31] A. S. Nair, R. Jose, Y. Shengyuan, and S. Ramakrishna, "A simple recipe for an efficient TiO2 nanofiber-based dye-sensitized solar cell.," *J. Colloid Interface Sci.*, vol. 353, no. 1, pp. 39–45, Jan. 2011.